Available online at www.sciencedirect.com
ScienceDirect
Journal of Power Sources 168 (2007) 282–287
JOURNAL OF POWER SOURCES
www.elsevier.com/locate/jpowsour

Short communication

High rate capability of the Mg-doped Li–Mn–O spinel prepared via coprecipitated precursor

Xiaoqing Wang *, Osamu Tanaike, Masaya Kodama, Hiroaki Hatori

Energy Storage Materials Group, Energy Technology Research Institute, National Institute of Advanced, Industrial Science and Technology (AIST), Tsukuba West, 16-1 Onogawa, Tsukuba, Ibaraki 305-8569, Japan

Received 20 December 2006; received in revised form 17 February 2007; accepted 23 February 2007
Available online 12 March 2007

Abstract

Coprecipitation was applied to prepare Mg–Mn hydroxide precursor for optimal synthesis of Mg-doped Li–Mn–O spinel. The as-obtained precursor was then mixed with LiOH followed by an annealing at 850 °C for 15 h. The spinel prepared from coprecipitated precursor can deliver over 100 mAh g^{-1} at a discharge rate as high as 10*C* (1.2 A g^{-1}) and retain 100% of the initial capacity in the 45th cycle while the spinel prepared directly from the as-purchased metal salts yields both smaller initial capacity and lower capacity retention after cycling. It was found that the crystallinity is higher and the charge transfer resistance is lower for the spinel prepared via coprecipitated precursor, which maybe resulted from the more homogeneous distribution of metal ion in such a spinel, than that in the spinel prepared from as-purchased reagents.

Keywords: Mn spinel; Rate capability; Coprecipitation; Homogeneous distribution; Crystallinity; Charge transfer resistance

1. Introduction

Li ion batteries with high energy density are possible high power sources for portable electronic devices and hybrid electric vehicle (HEV). Spinel $LiMn_2O_4$ is an attractive cathode material for Li ion batteries due to its low cost, nontoxity compared to the presently commercialized $LiCoO_2$ and a higher operation potential of 4 V than other current widely studied layered compound Li–Ni–Co–Mn–O and olivine structural $LiFePO_4$, etc. However, two problems exist in $LiMn_2O_4$ for high power applications. One is Mn dissolution, which has already been successfully solved by Yoshio and co-workers, where a two-step annealing method was employed to reduce surface area and oxygen deficiency, respectively [1]. The other problem is the rate capability of spinel. Its rate performance has been enhanced to some extent by alien metal doping [2] and metal oxide coating [3,4].

Among the doping elements, Mg has good electron conductivity and can also stabilize the host crystal structure [1,5], we select Mg to partially substitute for Mn^{3+} in spinel in order to promote the electron conductivity. On the other hand, also the focus of this study, coprecipitation is used to prepare Mn–Mg hydroxide for optimal synthesis of spinel aimed at achieving high rate capability. As a precursor synthesis method, coprecipitation has been recently drawing significant attention among worldwide energy storage material and battery researchers. Many research groups have successfully applied coprecipitation to obtain excellent cathode material based on Li–Ni–Co–Mn–O layered compounds for Li ion battery [6–8]. Some of these compounds are prepared from a coprecipitated mixed metal hydroxide precursor, in which the uniform disperse of each metal ion is available. We believe that a coprecipitated metal hydroxides precursor could contribute to improving the rate capability of Mn spinel. So far, only a few of analogic attempts have been made on synthesis of spinels [9–11]. However, none of these studies has been concerned with the effect of coprecipitated precursor on its rate capability. Hence, in this work, we applied coprecipitated precursor for the first time, to our best knowledge, to prepare Mg-doped Mn spinel in order to enhance its rate capability.

First, the mixed Mg–Mn hydroxide with a given ratio is prepared, and then the as-obtained precursor was calcined with addition of slightly excessive LiOH at high temperature to form a spinel structure. For comparison, another Mn spinel was also

* Corresponding author. Tel.: +81 29 8618712; fax: +81 29 8618712.
E-mail address: wxqzlq@yahoo.co.jp (X. Wang).

0378-7753/$ – see front matter © 2007 Elsevier B.V. All rights reserved.
doi:10.1016/j.jpowsour.2007.02.066

prepared directly from the purchased agent without any further treatment followed a same solid state reaction process. The former spinel from coprecipitated precursor shows much better rate capability at high discharge rate of 10*C* (1.2 A g^{-1}). The reasons accounting for the different rate capabilities have also been discussed in the following section considering the crystallinity and charge transfer resistance of two spinels.

2. Experimental

2.1. Synthesis

Sample A was prepared from coprecipitated precursor $(Mg_{0.05}Mn_{1.95})(OH)_2$, which was prepared as follows. Stoichiometric ratios of $MnSO_4{\cdot}5H_2O$ (Wako Pure Chemical Industries, 99% purity) and $MgSO_4$ (Kanto Chemicals, 98% purity) were completely dissolved into distilled water and then slowly dropped down into the NaOH solution with a pH value of 12 in a N_2 atmosphere at ambient temperature. The coprecipitated solid was dispersed rapidly by stirring the NaOH solution. The as-obtained suspension was filtered and washed three times with distilled water and then dried at 110 °C in air for overnight. A 3% excessive amount of $LiOH{\cdot}H_2O$ (compensation for possible Li loss during high temperature calcination) was mixed with the as-prepared precursor and preheated at 500 °C for 5 h and then calcined at 850 °C for 15 h in air. For comparison, sample B was prepared by heating a thoroughly ground mixture of $LiOH{\cdot}H_2O$:$MnSO_4{\cdot}5H_2O$:$(CH_3COO)_2Mg{\cdot}4H_2O$ with a same molar ratio of 1.03:1.95:0.05 following the same procedures as sample A: 500 and 850 °C/15 h. Both spinels were then reheated at 600 °C for 5 h to remove oxygen deficiency probably produced during 850 °C annealing.

2.2. Characterization

The contents of cations in both spinels were measured by inductively coupled plasma atomic analysis (ICP). The chemical compositions of samples A and B are $Li_{1.04}Mg_{0.045}Mn_{1.92}O_4$ and $Li_{1.07}Mg_{0.049}Mn_{1.88}O_4$, respectively, as listed in Table 1.

XRD was performed to examine the crystallinity of both spinels on an X-ray diffractometer (Rigaku, RTP 500) with a Cu Kα radiation.

The particle morphology of both spinels before and after prolonged cycling was observed using scanning electron microscopy (SEM, S-4700, Hitachi).

The charge–discharge experiments were conducted on a two-electrode screw cell consisting of a spinel cathode, a Li foil anode and an electrolyte of 1 M $LiPF_6$ in a 1:1 (in volume) mixture of ethylene carbonate (EC)/diethylene carbonate (DEC) (Tomiyama Pure Chemical). The spinel cathode was composed of 10 mg of spinel and 5 mg TAB (Teflonized acetylene black) as both a conductor and a binder on a stainless steel grid. Charge–discharge tests were carried out on multi-channel battery testers (Hokuto Denko, HJ1001SM8A) from 3.5 to 4.3 V at various current rates ranged from *C*/6 (20 mA g^{-1}) to 10*C* (1200 mA g^{-1}). In this work, *C* was defined as 120 mAh g^{-1}. Electrochemical impedance spectroscopic (EIS) studies were performed on a three-electrode glass cell, which consists of a spinel working electrode, containing 3 mg of Mn spinel and 2 mg TAB, a Li metal reference electrode and a Li metal counter electrode. The EIS tests were done on a multichannel VMP potentiostat/galvanostat (multichannel potentiostat/galvanostat VMP-80, Princeton Applied Research). The cell was charged to a given potential between 3.5 and 4.3 V before EIS tests. The frequency ranged from 200 kHz to 10 mHz and acoscillation amplitude was 10 mV.

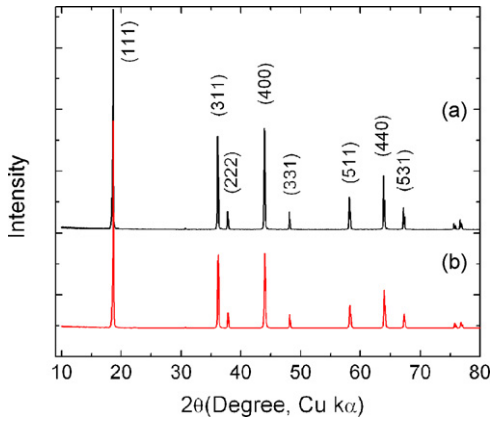

Fig. 1. XRD patterns of the as-prepared spinels: (a) sample A and (b) sample B.

3. Results and discussion

3.1. Crystal structure characterization

XRD patterns of two spinels were presented in Fig. 1. Both spinels are pure cubic phase without impurity. The lattice parameters are 8.239 and 8.226 Å for samples A and B, respectively (Table 1). It can be found that the intensity of each diffraction peak is higher for sample A than for sample B. In addition, full width at half maximum (FWHM) at diffraction peak (4 0 0) could be an important indicator for crystallinity of spinel [12]. As shown in Table 1, the FWHM at (4 0 0) for sample A is 0.18 smaller than that of sample B, which is 0.21. These results indicate that sample A has better-crystallized phase than sample B. Higher crystallinity is presumably resulted from the more uniform distribution of cation in the sample A thanks to the coprecipitated precursor compared to sample B.

Table 1
Chemical compositions, lattice parameters and FWHM at peak (4 0 0) of the two spinels

Sample	Precursor	Spinels compositions	Lattice parameter a_o (Å)	FWHM (4 0 0)
A	Coprecipitated precursor	$Li_{1.04}Mg_{0.045}Mn_{1.92}O_4$	8.239	0.18
B	As-purchased reagents	$Li_{1.07}Mg_{0.049}Mn_{1.88}O_4$	8.226	0.21

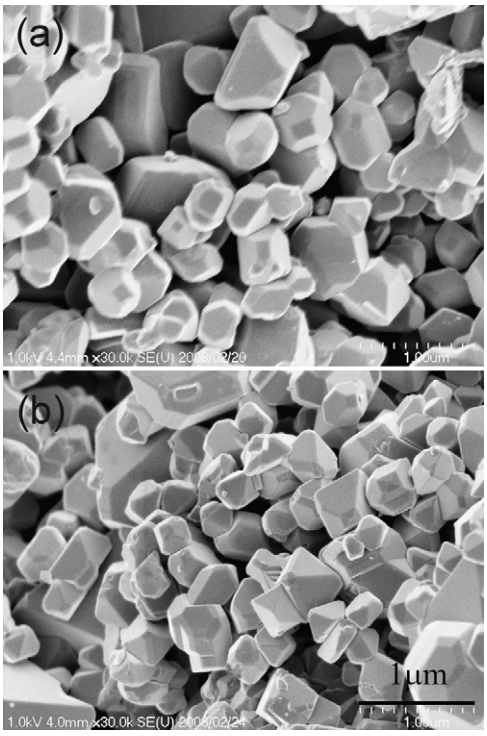

Fig. 2. SEM images of spinels: (a) sample A and (b) sample B.

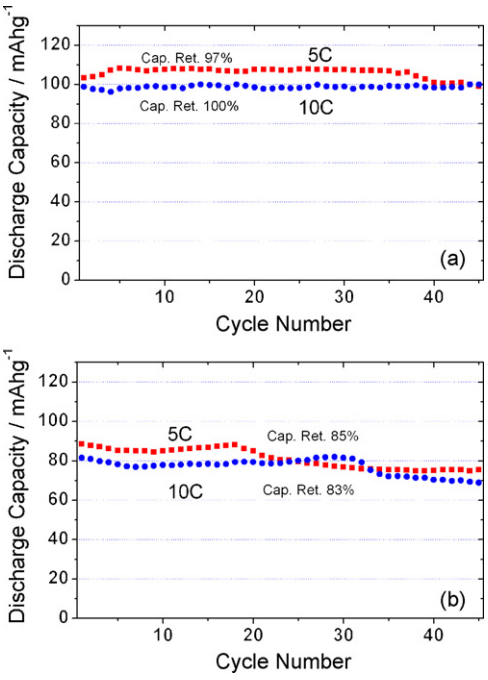

Fig. 4. Cycle life at high discharge rates of 5 and 10*C* for spinels: (a) sample A and (b) sample B, respectively; the charge rate is set at *C*/6 and the capacity retentions are also given in the figure.

3.2. Particle morphology

The particle morphology is demonstrated in Fig. 2. Both spinels have regular particle shape with similar size of ~1 μm, indicating that the particle morphology strongly depends on the heat-treating process regardless of different precursors used. This is in good agreement with the reported result [13].

3.3. Rate capability

Two spinels were electrochemically studied in the voltage range of 3.5–4.3 V under various discharge current rates (*C* rate) ranged from *C*/6 (20 mA g^{-1}) to 10*C* (1.2 A g^{-1}). Fig. 3 illustrates the plots of discharge capacities as a function of current rates. By careful observation and comparison, the following points can be found. (I) As described in Fig. 3, both spinels show a decreasing tendency in discharge capacity with increasing *C* rates. (II) Discharge capacities for spinel A, however, are much higher than that for spinel B at any *C* rates. It is noticeable that spinel A can provide a discharge capacity of over 100 mAh g^{-1} even at a rate as high as 10*C* (1.2 A g^{-1}). In contrast, sample B could only deliver about 60 mAh g^{-1} at 10*C*.

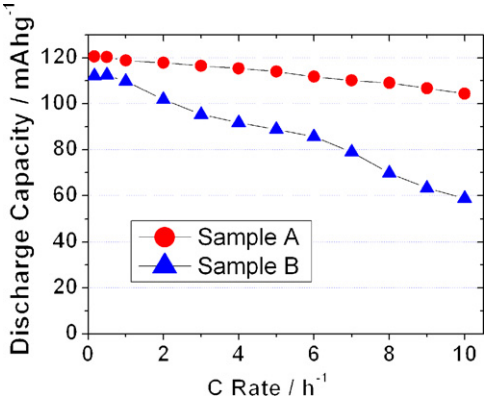

Fig. 3. Discharge capacities of spinels: (a) sample A and (b) sample B as a function of discharge rates of *C*/6 (20 mA g^{-1}) to 10*C* (120 mA g^{-1}); charge rate is fixed at *C*/6.

The cycleabilities of two spinels at high rates were also measured as shown in Fig. 4. The cell was discharged at 5*C* and 10*C* for 45 cycles. The charge rate was fixed at *C*/6. Sample A can still deliver 100 mAh g^{-1} after prolonged cycling with capacity retentions of 97 and 100% at 5*C* and 10*C*, respectively. However, sample B just remains 75 and 68 mAh g^{-1} in the 45th cycle, showing rather lower capacity retentions of 85 and 83% at 5*C* and 10*C*, respectively. Here, one may notice that sample B can give capacities of 81 mAh g^{-1} (1st cycle) and 68 mAh g^{-1} (45th cycle) at discharge rate of 10*C*, which is much higher than 60 mAh g^{-1} available at 10*C* in Fig. 3. This difference is caused from the different procedures of two experiments. The cell is discharged continuously at *C* rates varied from *C*/6 to 10*C* for 5 cycles, respectively, in the former test (Fig. 4b) and is cycled at 10*C* for 45 cycles in the latter test (Fig. 3). This difference also reflects the quicker capacity fading trend for sample B than sample A, consistent with the results in Fig. 4. The lower initial capacity of sample B than sample A is due to the slight Li excess in sample B. Both the capacity and the cycling property of sample A are dramatically superior to sample B. This should be resulted from the different precursor but not from the particle size since both samples show quite similar morphology in term of particle shape and particle size. To clarify the reasons

responsible for the different rate capabilities of two spinels, the following tests including ex situ XRD, ex situ SEM and EIS were carried out.

3.4. Ex situ XRD after cycling

After 45 cycles at high discharge rate of 5*C* or 10*C*, the cells were disassembled in an Argon-filled glove bag and rinsed with DMC. After dried at ambient temperature, the spinel electrodes were characterized in term of XRD measurement and SEM observation. Fig. 5 compares the ex situ XRD patterns of the spinel electrodes before and after 45 cycles at 10*C*. As can be seen, both electrodes show XRD patterns very close to that before cycling. The only difference caused by the repeated cycling at high rate is the slightly decreased intensities for sample B while no obvious variation for sample A can be found indicating that the crystal structures of both spinels are very stable and almost remain unaffected after the prolonged cycling at high discharge rate.

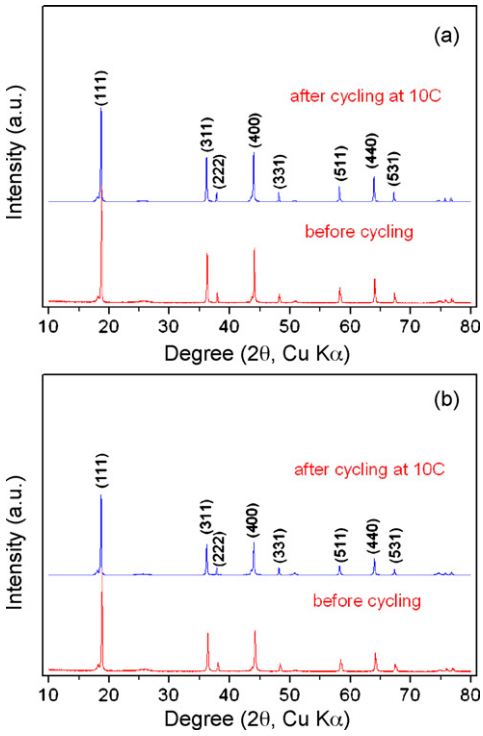

Fig. 5. Ex situ XRD patterns of two spinels after 45 cycles at a discharge rate of 10*C*.

3.5. Ex situ SEM images after cycling

The SEM images of the spinel electrodes after 45 cycles at discharge rate of 5*C* and 10*C* were illustrated in Fig. 6. In the case of sample A, one can find that there is almost no observable change in the morphology of spinel particle after cycled at 5*C* and only a few white spots appear on the surface of the spinel particle after cycled at 10*C*. Whereas, for sample B, many white spots form on the surface of the spinel particle when cycled at both 5*C* and 10*C*. The chemical composition of the white spots is still unclear at this stage. It is presumbly composed of Li-rich spinel or deposition of electrolyte decomposition. These phenomenons indicate that sample A has more stable surface, which could be associated with its higher crystallinity, than sample B. As for the possibility of deposition of Li-rich spinel, it is reasonable to assume that high crystallinity can provide per-

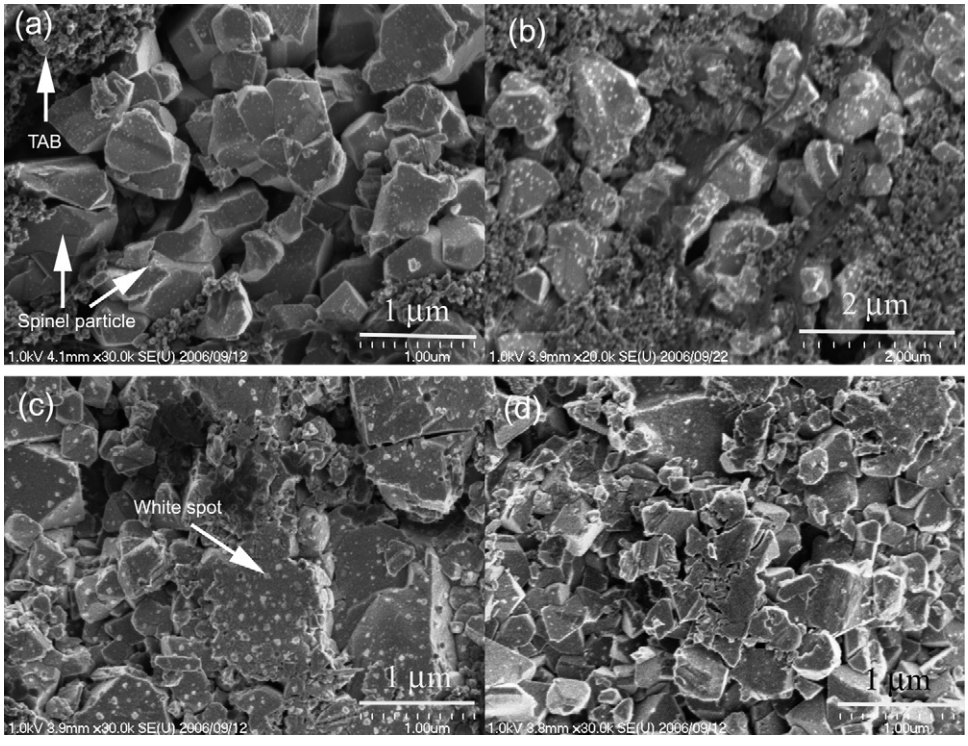

Fig. 6. Ex situ SEM images of cycled electrodes: (a and b) A and (c and d) B, both after 45 cycles at 5*C* and 10*C*.

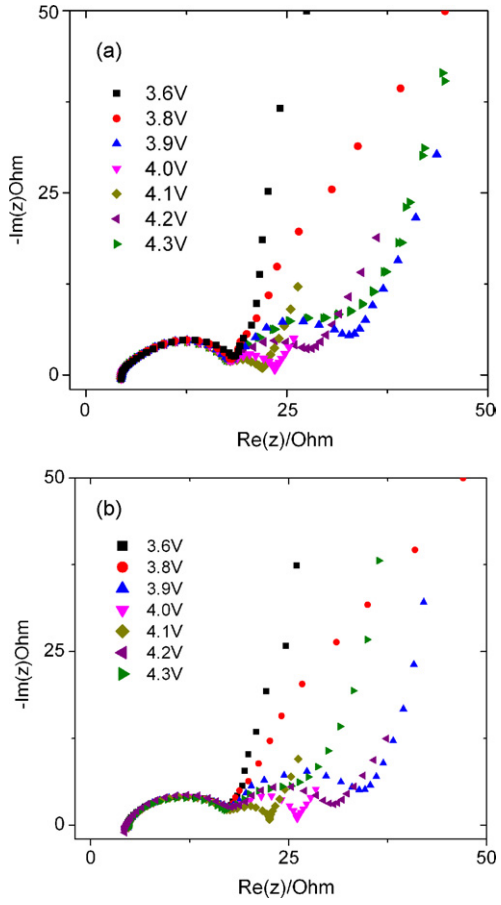

Fig. 7. Electrochemical impedance spectra of the as-prepared spinels: (a) A and (b) B at different charge states.

fect Li ion diffusion path inside particle, which, consequently, favors rapid Li ion diffusion and thus leads to excellent high rate capability. The higher the crystallinity, the better the high rate capability. For the sample with lower crystallinity, the Li ion diffuses much slowly inside particle while quickly in electrolyte and, therefore, more Li ion would accumulate on the surface of the electrode possibly resulting in formation of more white spots composed of Li-rich spinel.

3.6. EIS studies of uncycled spinel electrodes

Fig. 7 depicts the electrochemical impedance spectroscopy (EIS) for two spinels. The data were recorded at various potentials during Li deintercalation process (charging). As clearly shown in this figure, both spinels indicate one high-to-medium frequency semicircle (semicircle 1), one medium-to-low frequency semicircle (semicircle 2) and a low frequency sloping line. It is noticeable that the semicircle 1 is independent of potential; however, the semicircle 2 strongly relates to the potential, only clearly appearing at potentials beyond 3.8 V and below 4.3 V. These results are very similar to the reported data [14–18]. As for the EIS of Li intercalation cathode material, no uniform conclusion but several different interpretations exist, especially related to the semicircle 1. Hjelm and Lindbergh [14] have investigated the EIS for composite $LiMn_2O_4$ cathode on carbonized and non-carbonised aluminium current collector and thin film electrode $LiMn_2O_4$ on gold current collector. Two well-separated semicircles appear for the composite electrode on a non-carbonised current collector. In contrast, only one semicircle and a sloping line were observed for the composite electrode on a carbonized current collector and thin film electrode on gold. Therefore, the semicircle 1 was attributed to the contact between the current collector and the active electrode material and the semicircle 2 was due to the kinetics of the active electrode material. The absence of the semicircle 1 for the thin film electrode resulted from the improved electrical contact between the current collector and the active electrode material. Aurbach et al. claimed that the semicircle 1 is related to the Li ion diffusion in the surface film, possibly Li_2CO_3 [16]. In the present study, we consider the semicircle 1 is related to rather the electrode fabrication and cell assembly procedure than the active electrode material itself since both spinels show very similar semicircle 1. It maybe associated with the contact between current collector and active electrode material. Semicircle 2 could be ascribed to the Faradic charge transfer resistance coupled with relative double layer capacitance and the sloping line at low frequency represents the Li ion diffusion in the spinel electrode as many researchers claimed [16,18]. It is noteworthy that semicircle 2 varies with the potentials for both spinels. The diameter of this semicircle representative of the charge transfer resistance is calculated and plotted as a function of the potential in Fig. 8. As can evidently be seen, the charge transfer resistances of both spinels show a U-type tendency versus potential, which agrees well with the reported results [16,18]. Importantly, over the entire potential range, sample A has lower charge transfer resistance than sample B. This should be one critical reason responsible for the excellent high rate performance of sample A compared to sample B. The lower charge transfer resistance of sample A than sample B probably resulted from its higher crystallinity.

Based on the above results, it can be concluded that sample A has excellent rate capability compared to sample B. It is reasonable to speculate that the significant difference in the obtainable rate capabilities of two spinels must be associated with their

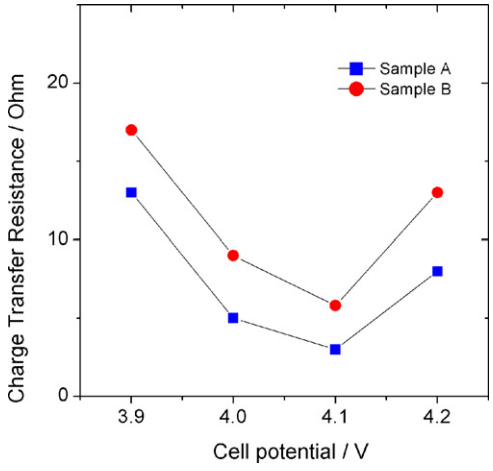

Fig. 8. Potential dependence of charge transfer resistance for spinels: (a) A and (b) B.

different crystallinity and charge transfer resistance. High crystallinity favors quick charge transfer and could enhance the electrode reaction and consequently lead to a high rate capability.

4. Conclusions

Two spinels were synthesized from different precursors, coprecipitated Mg–Mn hydroxides and the as-purchased metal salts, following the same heating treatment procedure. The former spinel shows both much higher capacity and more stable cycling ability even at quick discharge rate of 10*C* ($1.2\,A\,g^{-1}$) than the latter one. The former one can still deliver over $100\,mAh\,g^{-1}$ at 10*C* in the first cycle and retain 100% of the initial capacity after 45 cycles at 10*C* in contrast to the later one, which can give initial $81\,mAh\,g^{-1}$ at 10*C* with low capacity retention of 83% after 45 cycles. The reasons accounting for such a significant difference were attributed to the different crystallinity and charge transfer resistance in two spinels. The spinel prepared from coprecipitated precursor has both higher crystallinity and lower charge transfer resistance than the other spinel. This should be contributed by the uniform cation distribution in the coprecipitated precursor, which helps to form a high crystalline Mn spinel material and thereby a high rate capability. All these results confirm that we successfully improved the rate capability of Mg doped spinel by applying coprecipitation to prepare precursor.

References

[1] B. Deng, H. Nakamura, M. Yoshio, Electrochem. Solid State Lett. (2005) A171.
[2] Z. Bakenov, I. Taniguchi, Solid State Ionics 76 (2005) 1027.
[3] A.M. Kannan, A. Manthiram, Electrochem. Solid-State Lett. 5 (2002) A167.
[4] S.C. Park, Y.M. Kim, Y.M. Kang, K.T. Kim, P.S. Lee, J.Y. Lee, J. Power Sources 103 (2001) 86.
[5] R.J. Gummow, A. de Kock, M. Thackeray, Solid State Ionics 69 (1994) 59.
[6] M.E. Spahr, P. Novak, B. Schnyder, O. Haas, R. Nesper, J. Electrochem. Soc. 145 (1998) 1113.
[7] Y.C. Sun, C. Ouyang, Z.X. Wang, X.J. Huang, L.Q. Chen, J. Electrochem. Soc. 151 (2004) A504.
[8] S. Jouanneau, K.W. Eberman, L.J. Kranse, J.R. Dahn, J. Electrochem. Soc. 150 (2003) A1637.
[9] R.H. Li, F.Y. Gong, H. Lin, W.J. Wang, Ionics 11 (2005) 343.
[10] M. Wei, J. Zhang, W.S. Yang, M.L. Zhang, X. Duan, Chin. J. Inorg. Chem. 18 (2002) 713.
[11] X. Qiu, X. Sun, W. Shen, N. Chen, Solid State Ionics 93 (1997) 335.
[12] V. Manev, T. Faulkner, J. Engel, Proceedings of the HBC98 the First Hawaii Battery Conference, 1998, p. 228.
[13] Y. Xia, N. Kumada, M. Yoshio, J. Power Sources 90 (2000) 135.
[14] A.-K. Hjelm, G. Lindbergh, Electrochim. Acta 47 (2002) 1747.
[15] S.-J. Bao, Y.-Y. Liang, W.-J. Zhou, B.-L. He, H.-L. Li, J. Power Sources 154 (2006) 239.
[16] D. Aurbach, M.D. Levi, K. Gamulski, B. Markovsky, G. Salitra, E. Levi, U. Heider, L. Heider, R. Oesten, J. Power Sources 81–82 (1999) 472.
[17] D. Aurbach, K. Gamolsky, B. Markovsky, G. Salitra, Y. Gofer, U. Heider, R. Oesten, M. Schmidt, J. Electrochem. Soc. 147 (2000) 1322.
[18] A. Kobayashi, Y. Uchimoto, J. Phys. Chem. B 109 (2005) 13322.